J. Biochem. 2015;1–8 doi:10.1093/jb/mvv065 Journal of Biochemistry Advance Access published July 27, 2015 JB THE JOURNAL OF BIOCHEMISTRY

Mutagenesis study to disrupt electrostatic interactions on the twofold symmetry interface of *Escherichia coli* bacterioferritin

Received March 15, 2015; accepted May 26, 2015; published online June 26, 2015

Yu Zhang[1,2], Lijun Wang[1], Maziar S. Ardejani[3], Nur Fazlina Aris[4], Xun Li[1,2], Brendan P. Orner[3] and Fei Wang[1,2,*]

[1]College of Chemical Engineering, Nanjing Forestry University, Nanjing 210037, China; [2]Jiangsu Key Lab of Biomass-Based Green Fuels and Chemicals, Nanjing 210037, China; [3]Department of Chemistry, King's College London, London, SE1 1DB, UK; and [4]School of Life Sciences and Chemical Technology, Ngee Ann Polytechnic 599489, Singapore

*Fei Wang, College of Chemical Engineering, Nanjing Forestry University, Nanjing, Jiangsu 210037, People's Republic of China. Tel: +86-25-85427649, Fax: +86-25-85427649, email: hgwf@njfu.edu.cn

Ferritins and other cage proteins have been utilized as models to understand the fundamentals of protein folding and self-assembly. The bacterioferritin (BFR) from *Escherichia coli*, a maxi-ferritin made up of 24 subunits, was chosen as the basis for a mutagenesis study to investigate the role of electrostatic intermolecular interactions mediated through charged amino acids. Through structural and computational analyses, three charged amino acids R30, D56 and E60 which involved in an electrostatic interaction network were mutated to the opposite charge. Four mutants, R30D, D56R, E60H and D56R-E60H, were expressed, purified and characterized. All of the mutants fold into α-helical structures. Consistent with the computational prediction, they all show a lowered thermostability; double mutant D56R-E60H was found to be 16°C less stable than the wild type. Except for the mutant E60H, all the other mutations completely shut down the formation of protein cages to favour the dimer state in solution. The mutants, however, retain their ability to form cage-like nanostructures in the dried, surface immobilized conditions of transmission electron microscopy. Our findings confirm that even a single charge-inversion mutation at the 2-fold interface of BFR can affect the quaternary structure of its dimers and their ability to self-assemble into cage structures.

Keywords: bacterioferritin/electrostatic interaction/nanocage/self-assembly/site-directed mutagenesis.

Abbreviations: BFR, bacterioferritin; CD, circular dichroism; DLS, dynamic light scattering; SEC, size exclusion chromatography; TEM, transmission electron microscopy.

Protein cages are structures that are roughly spherical in shape, and enclose a central, hollow cavity. The ferritins, a family of protein cages, play a key role in iron sequestration and are evolutionarily ubiquitous among all kingdoms of life (*1–3*). Since the first ferritin was isolated from horse spleen by Laufberger in 1937 (*4*), ferritin proteins have been widely studied. The crystal structure of a ferritin was first resolved in 1991, which revealed the protein to be a 24-meric cage with octahedral symmetry (point group 432) (*5*). Similar to other ferritins, the exterior diameter of the *Escherichia coli* bacterioferritin (BFR) is ~12 nm and the interior cavity diameter is ~8 nm. The cavity, which can accommodate up to 4,500 iron atoms, typically contains the mineralized hydrate, Fe(III)O (*6*). Each monomer is made up of a four-helix bundle (A–D helices) with a short fifth helix (the E helix) at the C-terminus. In the octahedral cage structure, each subunit interacts with six surrounding monomers through three types of interfaces organized around 4-fold (C4), 3-fold (C3) and 2-fold (C2) symmetry axes (Fig. 1) (*7*). Given the relatively simple fold of ferritin monomers that are assembled into the octahedral 24-mer with C4, C3, C2 symmetry, these proteins can be adapted as a minimal model system for the study of protein–protein interactions that govern the formation of closed protein nanostructures.

Like a high majority of other ferritins, *E. coli* BFR is a homo-oligomer formed by self-assembly of identical monomers. We and others have demonstrated that the wild-type *E. coli* BFR populates two different oligomerization states, 24-mer (nanocage) and dimer, in solution (*9–11*). Previous study has shown that it is possible to shift this distribution of oligomers from 24-mer to dimer by single mutations to alanine at the C2 interface (*11*). Conversely, it has also been reported that computationally designed point mutations can stabilize the C2 interface in a way that favours the formation of higher oligomerization (nano-cage) state (*12*). We have also verified that a similar computational design strategy can be used to engineer BFR at its 3-fold symmetrical interfaces so that it solely self-assembles into the cage state (*13*). In the overall assembly mechanism of a maxi-ferritin, it has been proposed that the cage structure is constructed through a series of concentration-dependent association reactions involving a mixture of partially assembled subunits. These subunits include the dimer, the most highly populated species (*14*). Taking these observations together, it is clear that BFR's C2 interface plays an important role in the modulation of this protein's self-assembly, and the self-assembly can be manipulated through simple residue substitutions at this interface.

Ferritin has been used as model system to study the self-assembly of macromolecular complexes. In order

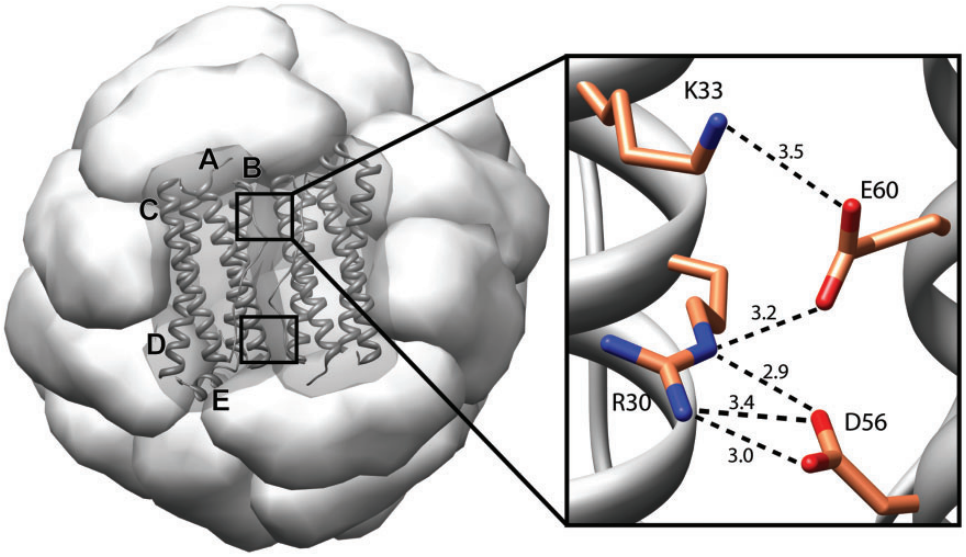

Fig. 1 BFR protein cage and four charged residues of interest. (*Left*) BFR protein cage viewed along the 2-fold symmetry axis. Protein monomer is a four-helix bundle architecture as exhibited. The interactions of interest are boxed. Note that they are related by the C2 symmetry axis. (*Right*) The expansion of one of these regions shows the interactions between four charged residues (K33, R30, E60 and D56). The heavy atom distances between the interaction groups are indicated in Å. The figure is generated using UCSF Chimera (*8*) (PDB ID: 1bfr).

to construct heteromeric protein cage with multiple functionalities by reassembling dissociated subunits, obtaining the Bfr monomer is the first essential step. In previous work, we demonstrated the importance of salt bridge formation and its significance in self-assembly of the BFR cage (*11*). It was found that residue R30 located at the C2 interface and which forms electrostatic interactions with D56 and E60, plays an important role in the self-assembly of the cage state (*11*). The mutant R30A disassembles into stable dimers in solution. Our analyses show that R30 is involved in a cluster of electrostatic interactions mainly with D56 and E60 (Fig. 1). This interaction cluster is part of the unified interaction network across the C2 interface (Supplementary Fig. S1) (*12*). It is hypothesized that charge-inversion mutations in this cluster of electrostatic interactions will have a detrimental effect on the stability of cage assembly. Will charge repulsion at C2 symmetry axes lead to the dissociation of ferritin nanostructure into monomers? To investigate this hypothesis, after inspection of *E. coli* BFR's crystal structure and computational analysis, we mutated the charged residues R30, D56, E60 to the oppositely charged amino acids to determine the role that these protein–protein interactions play in the self-assembly of the nano-cage structure.

Materials and Methods

Computational estimation of unfolding free energy using FoldX

The semi-empirical force field FoldEF as implemented in FoldX software (*15*) was used to calculate the free energy differences of all possible charge-inverted mutants. PDB entry 2vxi (*16*) was chosen for computational mutagenesis experiments because of all the BFR crystal structures it had the highest resolution at the time. The dimer was generated by deleting all the subunits except two chains, C and D, which are centred at a C2 symmetry axis. The RepairPDB protocol was used to minimize the energy of the structure. The side chains were rotated while the backbones were fixed and the buffer sulfate and heme ligands were removed. The repaired PDB file was then used with the BuildModel protocol to explore the changes in unfolding free energies (relative to that of the wild type) of the possible point mutants (at 298 K, pH 7.0, 50 mM ionic strength). The calculation for each mutant was repeated at least three times, the $\Delta\Delta G$ values were averaged and the standard deviation was calculated. In addition, these amino acids, R30, D56 and E60, were virtually mutated to alanine, so as to compare with the previous alanine scanning studies performed using a different computational approach (*11*).

Cloning of the mutant genes

All four mutants were constructed using QuikChange site-directed mutagenesis kit (Stratagene) with the BFR vector (*10*, *11*) as the template using the primers (Supplementary Fig. S2). The plasmids pET-32 Ek/LIC harbouring the respective gene inserts were obtained by miniprep and sequenced. The resulting sequences were aligned with the designed gene sequences using the Blast web tool that is available online: http://blast.ncbi.nlm.nih.gov/.

Protein expression and purification

Plasmids harbouring the desired genes were transformed into *E. coli* BL21 (DE3) (Novagen) cells by electroporation. Expression culture in 500 ml of LB supplemented with carbenicillin (50 μg/ml) was not induced with IPTG (0.4 mM) until OD_{600} reached approximately 0.4–0.6 and further incubated (30°C, 3 h). The cells were harvested by centrifugation and lysed (300 mM NaCl, 50 mM NaH_2PO_4, 10 mM imidazole, pH 8.0) by sonication. Proteins produced using pET-32 Ek/LIC contain a number of N-terminal fusion tags (Poly-Histidine, thioredoxin and S-tag, respectively) followed by the enterokinase cleavage site right before the N-terminal of target protein to permit affinity purification and to improve solubility. Once the tagged proteins were isolated on affinity resin, the fusion tags were to then be removed by enzymatic digestion. The soluble protein was applied to Ni-NTA resin (QIAGEN) and eluted by affinity tag cleavage following incubation with enterokinase (5 ul, 2.0 μg/ml, 4°C, 36 h). The protein was concentrated via ultrafiltration (Sartorius Vivaspin 6) and further purified by size exclusion chromatography (SEC). The final purity of the protein was determined by SDS-PAGE electrophoresis (Supplementary Fig. S3).

SEC

The purified proteins were subjected to SEC performed on an ÄKTAFPLC™ (GE Healthcare) system using a Superdex 200 10/300 GL gel filtration column pre-equilibrated with running buffer (50 mM NaH_2PO_4, 150 mM NaCl, pH 7.0). All the SEC experiments were conducted at 4°C with a flow rate 0.5 ml/min (Fig. 3A).

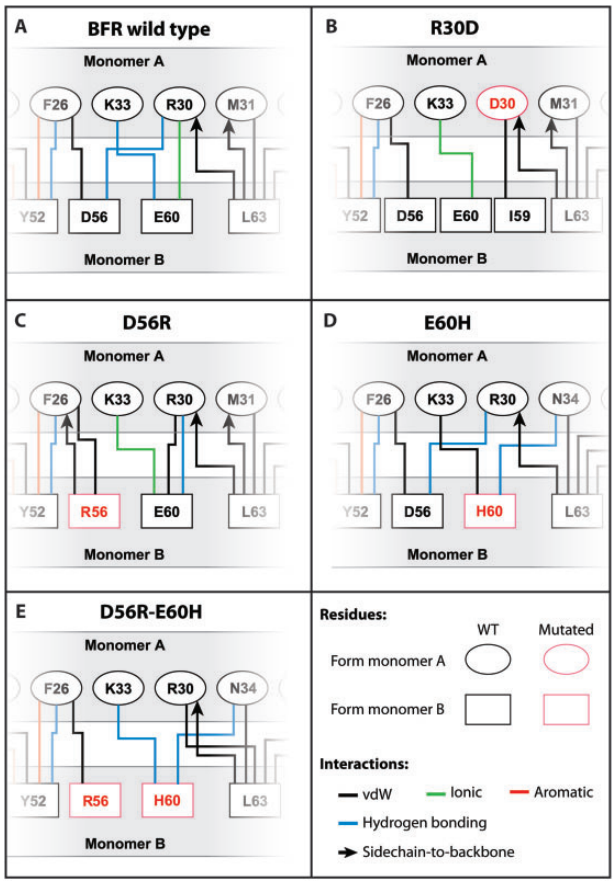

Fig. 2 The predicted effect of mutations on the interaction networks at the C2 interface. The inter-residue interaction network involved in electrostatic interactions across the C2 interface of BFR is composed of R30, K33, D56 and E60. Residues from monomer A and B are, respectively, shown in oval and squares. The mutants involved in the electrostatic interaction cluster are highlighted in red ovals or squares. Side-chain-to-side-chain interactions appear as lines and backbone-to-side-chain interactions are depicted as arrows pointing from the backbone to the side-chain. The contact maps were generated using Aquaprot (*17*) with the minimized crystal structure of BFR and mutants.

The column was previously calibrated using six well-characterized proteins as standards (GE Biosystems Calibration Kit) (*10*).

DLS

Sample concentration was determined by BCA kit (Novagen) and diluted to 200 μg/ml with phosphate buffer (50 mM NaH_2PO_4, pH 7.2). Dynamic light scattering (DLS) analysis was carried out on a 90Plus particle size analyzer instrument (Brookhaven Instruments Ltd.) using a 0.5 cm path length cuvette. Three data sets were collected at 25°C for each protein. The hydrodynamic diameter was averaged from the three replicates (Fig. 3B). The polydispersity was less than 20% for all samples.

Native PAGE

A 7% gel was run using 20 μg for all the proteins and was stained with Coomassie Blue. Tris-glycine electrophoresis buffer at pH 8.3 was used as gel running buffer.

TEM

The purified protein (10 μl, ~20 μg/ml) was stained using uranyl acetate (1% w/v). Formvar carbon grid (300 mesh) was used. Transmission electron microscopy (TEM) data was obtained using a Joel JEM-1400 transmission electron microscope operating at 100 keV. TEM micrographs were analyzed using ImageJ (NIH). For each protein, 100 particles were measured (Fig. 4).

Temperature-dependent CD analysis

The protein solutions were equilibrated in phosphate buffer (50 mM NaH_2PO_4, pH 7.2) through extensive dialysis. Protein concentrations were determined by BCA (Novagen) and the solution was diluted (70 μg/ml) with phosphate buffer (50 mM NaH_2PO_4, pH 7.2). CD spectra were collected on a BioLogic MS-500 spectropolarimeter using a 2 mm quartz cell at 222 nm, 1°C intervals (3 min) over a temperature range of 25–95°C. Once the protein solutions reached 95°C, they were cooled slowly to 25°C over 20 min, and the resulting spectra were compared to the spectra obtained at 25°C before thermal unfolding. At least three replicates were performed (Fig. 5).

Results

Computational selection of interfacial residues for mutagenesis with FoldX

Amino acid residues R30, D56 and E60 that form an electrostatic interaction cluster at the dimer interface were mutated *in silico* so that the opposite charge was achieved at each position. The charge-inversion mutations may interfere with the wild-type salt bridges and hydrogen bonds at the C2 interface and cause repulsion. Hence, it was hypothesized that such mutations would destabilize the protein complex. As anticipated, most of the $\Delta\Delta G$s predicted using FoldX for such mutations are positive (Supplementary Table S1), denoting the fact that these mutations would have a destabilizing effect on the structure of C2 interface (*18*). Subsequently, the virtual mutants with the highest positive $\Delta\Delta G$, R30D, D56R, E60H and D56R-E60H were selected for expression and further characterization. Surprisingly, most of charge-inversion mutations of E60 were not predicted to have a destabilizing effect (Supplementary Table S1). A possible explanation for this will be discussed in the next section where we analyze how these charged residues interact at C2 protein–protein interface.

Effect of the mutations on the interaction network of BFR's C2 interface

The inter-residue interaction network across the C2 interface of BFR is rather complex. This network can be simplified as a two-dimensional representation where interfacial residues act as 'nodes' and cross-monomer interactions form 'edges' linking one interface residue to its interaction partner from neighbouring monomer (Supplementary Fig. S1). Such an analysis reveals that the wild-type interaction network of the C2 interface forms a single extended network to which every interfacial residue is connected by at least one type of interaction (Fig. 2). Near the centre of this network is the localized cluster of electrostatic interactions composed of R30, K33, D56 and E60 (Fig. 2A). A salt-bridge and a hydrogen bonding interaction link R30, respectively, to E60 and D56. These interactions coincide with E60 and K33 interacting through hydrogen bonding to form the electrostatic cluster. Three of the charge-inversion mutations, R30D and D56R and the double mutation D56R-E60H, disturb this electrostatic cluster and break the otherwise unified interaction network at the C2 interface into separate parts. However, the E60H mutation (Fig. 2D) rearranges the C2 interaction network in a way that its coherence is maintained. Based on these

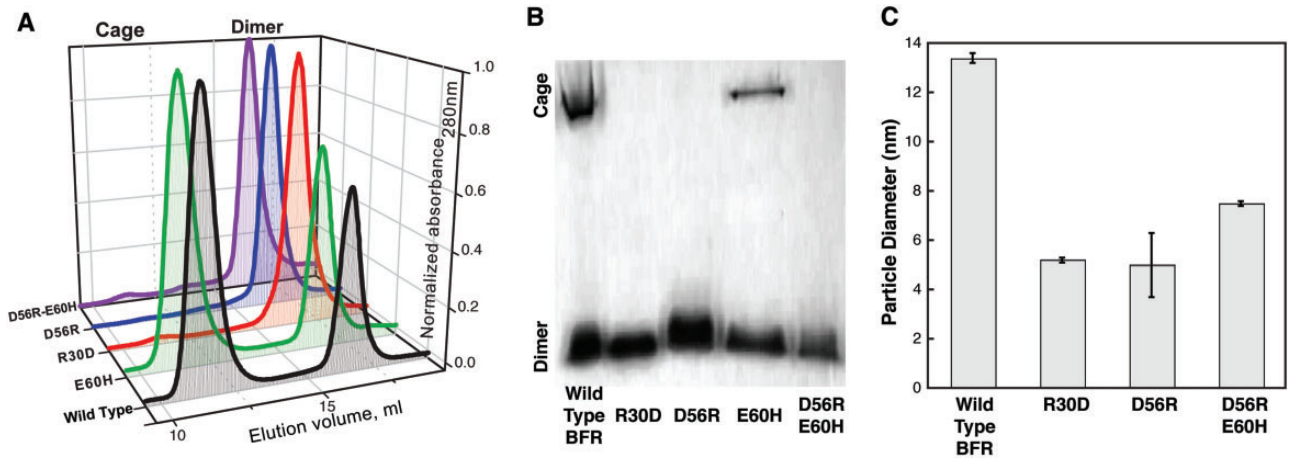

Fig. 3 Oligomerization preference of mutants characterized by SEC, native PAGE and DLS. All the mutants form dimer solely in solution except BFR E60H. (**A**) SEC chromatograms of BFR wild type and four mutants showing that three mutants form only dimer in these conditions. The purified proteins were analyzed using a Superdex 200 10/300 GL gel filtration column pre-equilibrated with running buffer (50 mM NaH_2PO_4, 150 mM NaCl, pH 7.0). All the SEC experiments were conducted at protein concentration ~0.6 mg/ml, 4°C with a flow rate 0.5 ml/min. (**B**) Native PAGE of BFR wild type and four mutants. A 7% gel was run using 20 μg for all the proteins and was stained with Coomassie Blue. (**C**) Hydrodynamic diameters for proteins as measured by dynamic light scattering. Sample concentration was 200 μg/ml in phosphate buffer. Three data sets were collected at 25°C for each protein. The hydrodynamic diameter was averaged from the three replicates. The polydispersity was less than 20% for all samples. Error bars represent the standard deviation.

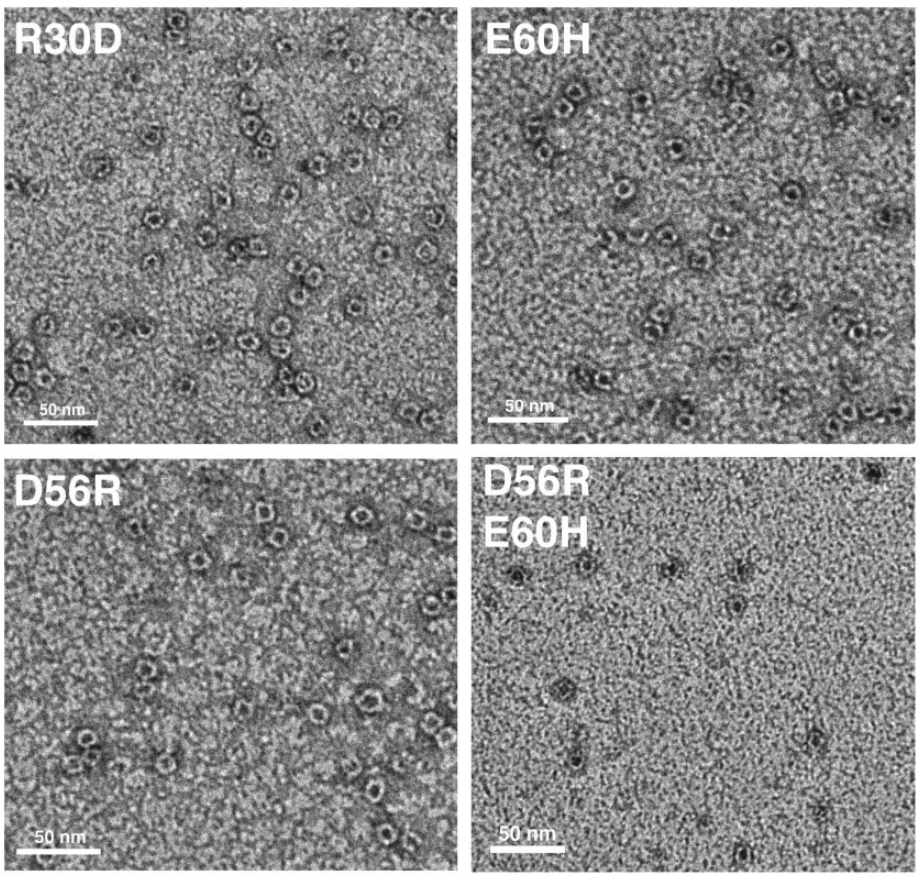

Fig. 4 TEM images of four BFR-derived mutants. All four BFR-derived mutants can form nano-cages under TEM conditions. The purified protein (10 μl, ~20 μg/ml) was stained using uranyl acetate (1% w/v) and loaded on formvar carbon grid (300 mesh). For each protein, 100 particles were measured. Scale bars indicate 50 nm.

analyses, it can be inferred that R30D, D56R and D56R/E60H mutations will possibly have a more detrimental effect on the stability and self-assembly of BFR than will E60H.

Protein expression and purification

Plasmids harbouring the desired mutations, prepared via site-directed mutagenesis using a BFR construct as a template, were verified by sequencing. All the

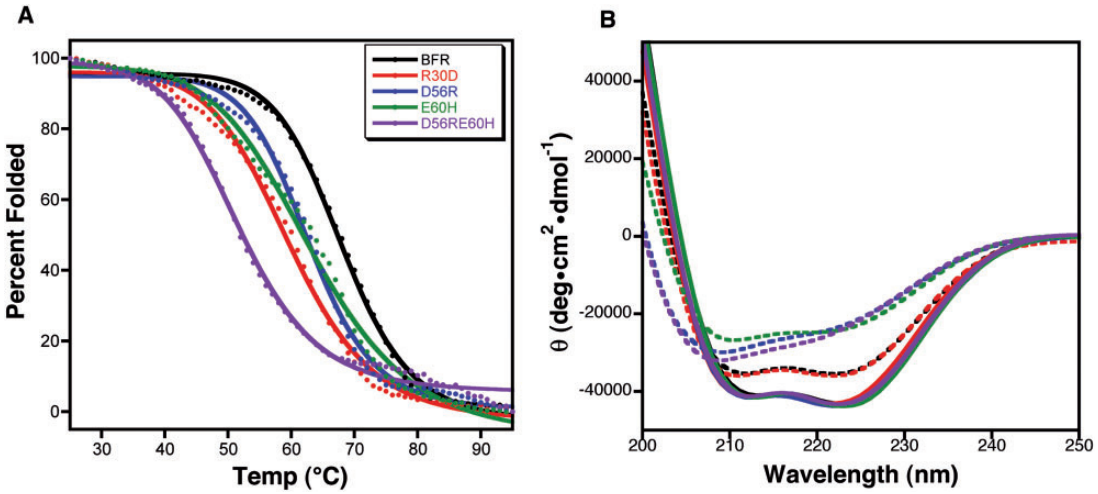

Fig. 5 The role mutation plays in the thermal stability and folding reversibility of four charged BFR. Protein concentrations were determined by BCA method and the solution was diluted to 70 μg/ml with phosphate buffer 50 mM NaH_2PO_4, pH 7.2. (**A**) Thermal transitions of the four charged BFR mutants were monitored by CD at 222 nm. Data were collected at 1°C intervals over a temperature range of 25–95°C. The solid lines are the fit and the dotted lines are the data. Data are the average of at least three replicates. (**B**) CD spectra of the BFR derivatives before denaturation (solid lines) and after slow cooling post-thermal denaturation (dashed lines). Once the protein solutions reached 95°C, they were cooled slowly to 25°C over 20 min. The resulting spectra were compared to the spectra obtained at 25°C before thermal unfolding. The colouring follows that of the left. Data are the average of at least three replicates.

mutations were successfully introduced into the expression vector. A series of SDS-PAGE gels were carried out to verify each step of the gene expression and protein purification procedure. The gels (Supplementary Fig. S3) demonstrate that all four charge-inversion mutants of BFR are expressed as soluble proteins, and pure protein bands appear as ~19 kD in size. Therefore, SDS-PAGE analyses have verified that the target proteins were successfully purified.

Size exclusion chromatographic analysis of BFR assembly in solution

The wild-type protein and those bearing charge-inversion mutations were analyzed by SEC (Fig. 3A). The wild-type BFR, consistent with the literature, forms a mixture of 24-mer and dimer (*10*, *11*). The E60H mutant of BFR exists in a similar ratio as the wild-type protein, while the other mutants (R30D, D56R and D56R-E60H) were observed to form a homogenous population of a lower order complex corresponding to dimer. This observation, taken together with the FoldX prediction of subtle changes in the stability and interaction networks, suggests that E60H mutation indeed has very little effect on the stability and overall structure of dimer and cage (Fig. 1). However, these results confirm that even a single charge-inversion mutation at C2 interface can affect the quaternary structure of the dimers and their ability to self-assemble into cage structures.

Oligomerization preference of mutants characterized by native PAGE and DLS

Native PAGE electrophoresis was performed to further confirm the oligomerization preference of the designed mutants. Consistent with the SEC experiment, for only the E60H mutant was a band corresponding to the 24-mer oligomerization state observed. All the other mutants generated bands corresponding to wild-type dimer (Fig. 3B).

Protein samples were characterized further using DLS to determine whether the three mutants, R30D, D56R, D56R-E60H, form 24-mer in solution. Comparison of the DLS data for the three mutants and wild-type BFR showed that these mutants form particles that are smaller than BFR (Fig. 3C), supporting the native electrophoresis and SEC observations.

TEM analysis of protein assembly

The proteins were further analyzed using TEM to determine whether each possessed the ability to assemble into a nanocage state. We have noted in the past that some protein cage mutants that are crippled in their ability to form the cage state in solution generate TEM-observable cages (*11*, *19*). This observation was attributed to the evaporated and surface-immobilized conditions required for TEM may be acting to force unfavourable cages together. Consistent with this previous observation, electron micrographs of the proteins from the current study indicated that they all have the ability to form cage under TEM forcing conditions (Fig. 4). Image analysis of the micrographs indicates that the size of the native protein structures are comparable to those described in the literature (*20*) (Table I). These results further underline our caveats with using TEM as a sole diagnostic of assembly in these systems.

Analysis of secondary structure and thermal stability via temperature-dependent CD

Characterization of the designed mutants using circular dichroism (CD) demonstrated they all fold into α-helical structures as evidenced by the spectral minima at 208 and 222 nm. All the mutants exhibit similar secondary structure as compared to the wild-type BFR. This suggests that mutations at the 2-fold symmetry axis do not have a noticeable effect on

the helicity and, most likely, the tertiary structure of the protein.

The thermal stability and folding reversibility of the BFR mutants were analyzed by heating the samples beyond denaturation, followed by gradual cooling to the starting temperature, and re-measuring the secondary structure. Despite having a depressed stability, R30D exhibited a similar thermal folding reversibility as wild-type BFR (Fig. 5). The largest reduction in reversibility is observed for E60H, which may be due to aggregation kinetically blocking the mutant from returning to the folded state. The double mutant D56R-E60H showed the lowest thermal stability with an unfolding mid temperature 16°C less than that of wild type. The fact that D56R-E60H has the lowest thermal stability is not fully consistent with the computationally calculated ΔΔGs where R30D mutant was predicted to have the lowest thermostability (Table II). This slight ranking discrepancy between the predicted and measured stability may arise from the dynamic effects that are beyond the prediction limits of computational method used here. It is worth mentioning that there is a lack of correlation between thermal stability and cage formation especially at C2 interfaces (*12*) reflecting dynamic properties of these interfaces that has yet to be unraveled. The mutants D56R and the double mutant D56R-E60H, had similar CD spectra after denaturation, with little signal at 222 nm indicating greatly reduced amount of α-helix.

The positive ΔΔG values calculated from FoldX indicate changes in the unfolding free energy between the wild type and the mutant; the higher the ΔΔG value, the greater the destabilizing effect of mutation on the dimer structure. Consistent with the computational calculation, all the mutants showed lower thermostability compared to the wild-type BFR. Interestingly, the mutation E60H, which is estimated to impose little destabilizing effect by the virtual mutation experiment, is indeed the least destabilizing as evidenced by thermal unfolding monitored by CD. This reflects the applicability of computational predictions for the engineering of such complex interactions in this system.

Table I. Average particle diameters of BFR and its charge-reversed mutants

Mutants	Particle diameter (nm)	SD (nm)
BFR wild type	14.3	1.0
R30D	12.1	0.8
D56R	12.1	0.7
E60H	13.0	1.1
D56R-E60H	10.8	0.9

Particle diameter of BFR wild type is taken from the reference (*11*). For each mutant, 100 particles were measured using ImageJ.

Discussion

The octahedrally symmetric *E. coli* bacterioferritin, BFR, was used in this study to understand the role that electrostatic interactions at the C2 interface play in the stability and self-assembly of the nano-cage structure. The natively monomeric form of ferritin has as of yet never been observed and strong evidence has indicated that metastable dimeric conformers are the intermediate structures for the multistep self-assembly ferritins (*7*, *9*, *10*). Careful scrutiny of these dimeric intermediates and the structural transition between them is essential for understanding and controlling ferritin self-assembly. It is also found that the association of ferritin subunits is pH-dependent, which means that the nano-cage structure can be shifted to monomer in acidic condition and be restored at neutral pH (*21*). Using this disassembly/reassembly approach, Douglas *et al.* (*22*) subjected two types of ferritin cages to pH-mediated transition and successfully constructed chimeric protein cages. Lin (*23*) employed the disassembly/reassembly nature as the driving force to load multiple motifs on a heavy-chain ferritin protein cage to build protease-sensitive probes. However, *E. coli* BFR suffers from low stability in acidic conditions and cannot be restored at natural pH (data not shown).

It has been demonstrated in previous work that the structure of BFR's C2 interface plays an important role in cage state self-assembly (*11*, *12*). In addition, it has been shown previously that residue R30, which forms electrostatic interactions with D56 and E60 at the C2 interface, plays an essential role in protein stability and cage assembly. Therefore, to further scrutinize electrostatic interactions in this protein with the long-term goal of obtaining the folded monomeric subunit of BFR in native conditions, the salt bridges at the C2 symmetry interface were manipulated. Hence, three charged residues R30, D56 and E60, identified by computational analysis and inspection of the crystal structure, were mutated to residues of the opposite charge to determine the role electrostatic interactions play in the self-assembly of the cage structure. After cloning, expression and purification, we found that all four mutants cooperatively fold into α-helical structures

Table II. Solution assembly state, melting temperature and ΔΔG unfolding free energy of charge-reversed mutants of BFR

Proteins	Assembly state[a]	T_m (°C) [a]	ΔT_m (°C)	$\Delta\Delta G_{calc.}$ [b] (kcal/mol)
BFR wild type	24-mer and Dimer	68.1		
R30D	Dimer	59.9	−8.2	12.5
D56R	Dimer	62.8	−5.3	6.8
E60H	24-mer and Dimer	63.3	−4.8	1.3
D56R-E60H	Dimer	51.7	−16.4	8.5

[a]Data are taken from Figs 3 and 5.
[b]Unfolding free energy calculated by FoldX is taken from Supplementary Table S1.

with lowered thermostability as evidenced by temperature-dependent CD. Furthermore, three mutants, R30D, D56R and D56RE60H only form dimers in solution with no observation of the cage or monomer states.

Comparing this work to the previously reported alanine scanning mutagenesis study, among the selected amino acid residues along the 2-fold axis, R30 and D56 appear to play the largest role in assembly and stability (*11*). It is interesting that two mutations of R30, R30D presented here and the previously reported R30A, although both form solely dimers in solution, display opposite thermostability compared to the wild-type BFR. The R30A mutant is more thermally stable and R30D is less stable than the wild-type protein. It is intriguing how the subtle structural difference between these two types of dimers could result in such variation in stability. Charge-inversion mutations involving D56 (D56R and D56R-E60H) completely shut down the formation of 24-mer and exhibit only dimers in solution. In contrast, D56A and D56A-E60A mutations, reported in the previous alanine scanning mutagenesis study, form mixtures of 24-mer and dimer in solution, indicating they have a subtle effect on the oligomerization state of nano-cage structure. Although hydrogen bonds and salt bridge interactions that are predicted to control the formation of dimers may be destroyed by mutation to opposite charges, the dimer still remains. And, this is not surprising because although more specific, the main role of electrostatic interactions is to fine-tune protein-protein interactions while protein self-assembly is mainly driven by less specific hydrophobic interactions (*24*). Therefore, it may not be very realistic to expect the disruption of an entire protein-protein interface just through few charge-inverting mutations.

As mentioned above, it has often been suggested that a dimeric subunit is a major intermediate in the ferritin mechanism of assembly (*14*, *25*, *26*). The productive form of this dimer has been assumed to be similar to the one that exists at the 2-fold axis in the cage (*11*). However, in this current study we have shown how manipulating the 2-fold symmetry related protein-protein interface can result in destabilization of the cage with no disruption of the dimer. In addition, through the course of attempting to rationally stabilize the BFR cage, we previously generated, by manipulating the 2-fold interface, a protein that was more thermally stable. This protein however formed more dimer and less cage than the wild type. Taking all these observations, there are a number of possible explanations: (i) the mutations could be inducing a conformational change within the monomer which changes the protein surface not involved in the dimer. This may be unlikely because of the similarities in the CD spectra; (ii) the dimer geometry could be altered resulting in a tighter dimer interaction but a dimer that cannot fit into an assembling cage. We have proposed this previously and refer to it as the 'Arch and Keystone Hypothesis' in that it resembles the alteration of the relative outer angles of a keystone to influence the final geometry of an architectural arch (*12*); (iii) the dimer assembly intermediate is not formed around the 2-fold symmetric interface. In fact, this dimer could or could not be an immediately obvious dimer deduced from inspection of the fully assembled cage. This final possibility could be probed by adopting a geometry-specific cross-linking detection strategy, like bipartite FlAsH, to monitor assembly at specific interfaces (*27*).

Supplementary Data

Supplementary Data are available at *JB* Online.

Funding

This research was supported by the National Natural Science Foundation of China (31200564 to Y.Z., 31170537 to F.W., 31270612 to X.L.) and a NJFU startup grant (YJ2012-05) as well as the Priority Academic Program Development of Jiangsu Higher Education Institutions (PAPD). B.P.O. was partially supported by Marie Curie CIG PCIG13-GA-2013-618538.

Conflict of Interest

None declared.

References

1. Andrews, S. C., Arosio, P., Bottke, W., Briat, J. F., Vondarl, M., Harrison, P. M., Laulhere, J. P., Levi, S., Lobreaux, S., and Yewdall, S. J. (1992) Structure, function, and evolution of ferritins. *J. Inorg. Biochem.* **47**, 161–174
2. Harrison, P. M. and Arosio, P. (1996) Ferritins: molecular properties, iron storage function and cellular regulation. *Bba Bioenergetics* **1275**, 161–203
3. Andrews, S. C. (2010) The ferritin-like superfamily: evolution of the biological iron storeman from a rubrerythrin-like ancestor. *Biochim. Biophys. Acta* **1800**, 691–705
4. Laufberger, V. (1937) Sur la cristallisation de la ferritine. *Bull. Soc. Chim. Biol.* **19**, 1575–1582
5. Lawson, D. M., Artymiuk, P. J., Yewdall, S. J., Smith, J. M. A., Livingstone, J. C., Treffry, A., Luzzago, A., Levi, S., Arosio, P., Cesareni, G., Thomas, C. D., Shaw, W. V., and Harrison, P. M. (1991) Solving the structure of human H-ferritin by genetically engineering intermolecular crystal contacts. *Nature* **349**, 541–544
6. Theil, E. C. (1987) Ferritin: structure, gene regulation, and cellular function in animals, plants, and microorganisms. *Annu. Rev. Biochem.* **56**, 289–315
7. Zhang, Y. and Orner, B. P. (2011) Self-assembly in the ferritin nano-cage protein superfamily. *Int. J. Mol. Sci.* **12**, 5406–5421
8. Pettersen, E. F., Goddard, T. D., Huang, C. C., Couch, G. S., Greenblatt, D. M., Meng, E. C., and Ferrin, T. E. (2004) UCSF chimera - A visualization system for exploratory research and analysis. *J. Comput. Chem.* **25**, 1605–1612
9. Andrews, S. C., Smith, J. M. A., Hawkins, C., Williams, J. M., Harrison, P. M., and Guest, J. R. (1993) Overproduction, purification and characterization of the bacterioferritin of Escherichia Coli and a C-terminally extended variant. *Eur. J. Biochem.* **213**, 329–338

10. Fan, R., Boyle, A. L., Cheong, V., Ng, S. L., and Orner, B. P. (2009) A helix swapping study of two protein cages. *Biochemistry* **48**, 5623–5630
11. Zhang, Y., Raudah, S., Teo, H., Teo, G. W. S., Fan, R. L., Sun, X. M., and Orner, B. P. (2010) Alanine-shaving mutagenesis to determine key interfacial residues governing the assembly of a nano-cage maxi-ferritin. *J. Biol. Chem.* **285**, 12078–12086
12. Ardejani, M. S., Li, N. X., and Orner, B. P. (2011) Stabilization of a protein nanocage through the plugging of a protein-protein interfacial water pocket. *Biochemistry* **50**, 4029–4037
13. Ardejani, M. S., Chok, X. L., Foo, C. J., and Orner, B. P. (2013) Complete shift of ferritin oligomerization toward nanocage assembly via engineered protein-protein interactions. *Chem. Commun.* **49**, 3528–3530
14. Gerl, M. and Jaenicke, R. (1987) Mechanism of the self-assembly of apoferritin from horse spleen. Cross-linking and spectroscopic analysis. *Eur. Biophys. J.* **15**, 103–109
15. Schymkowitz, J., Borg, J., Stricher, F., Nys, R., Rousseau, F., and Serrano, L. (2005) The FoldX web server: an online force field. *Nucleic Acids Res.* **33**, W382–W388
16. Littlechild, J. A., Willies, S. C., Isupov, M. N., and Garman, E. F. (2009) The binding of haem and zinc in the 1.9 angstrom X-ray structure of Escherichia coli bacterioferritin. *J. Biol. Inorg. Chem.* **14**, 201–207
17. Guerois, R., Nielsen, J. E., and Serrano, L. (2002) Predicting changes in the stability of proteins and protein complexes: a study of more than 1000 mutations. *J. Mol. Biol.* **320**, 369–387
18. Reichmann, D., Cohen, M., Abramovich, R., Dym, O., Lim, D., Strynadka, N. C., and Schreiber, G. (2007) Binding hot spots in the TEM1-BLIP interface in light of its modular architecture. *J. Mol. Biol.* **365**, 663–679
19. Zhang, Y., Fu, J., Chee, S. Y., Ang, E. X., and Orner, B. P. (2011) Rational disruption of the oligomerization of the mini-ferritin *E. coli* DPS through protein-protein interface mutation. *Protein Sci.* **20**, 1907–1917
20. Grant, R. A., Filman, D. J., Finkel, S. E., Kolter, R., and Hogle, J. M. (1998) The crystal structure of Dps, a ferritin homolog that binds and protects DNA. *Nat. Struct. Biol.* **5**, 294–303
21. Santambrogio, P., Levi, S., Arosio, P., Palagi, L., Vecchio, G., Lawson, D. M., Yewdall, S. J., Artymiuk, P. J., Harrison, P. M., Jappelli, R., and Cesareni, G. (1992) Evidence that a salt bridge in the light chain contributes to the physical stability difference between heavy and light human ferritins. *J. Biol. Chem.* **267**, 14077–14083
22. Kang, S., Oltrogge, L. M., Broomell, C. C., Liepold, L. O., Prevelige, P. E., Young, M., and Douglas, T. (2008) Controlled assembly of bifunctional chimeric protein cages and composition analysis using noncovalent mass spectrometry. *J. Am. Chem. Soc.* **130**, 16527–16529
23. Lin, X., Xie, J., Zhu, L., Lee, S., Niu, G., Ma, Y., Kim, K., and Chen, X. (2011) Hybrid ferritin nanoparticles as activatable probes for tumor imaging. *Angew. Chem. Int. Ed. Engl.* **50**, 1569–1572
24. Jaremko, M., Jaremko, L., Kim, H. Y., Cho, M. K., Schwieters, C. D., Giller, K., Becker, S., and Zweckstetter, M. (2013) Cold denaturation of a protein dimer monitored at atomic resolution. *Nat. Chem. Biol.* **9**, 264–270
25. Stefanini, S., Vecchini, P., and Chiancone, E. (1987) On the mechanism of horse spleen apoferritin assembly - a sedimentation-velocity and circular-dichroism study. *Biochemistry* **26**, 1831–1837
26. Gerl, M., Jaenicke, R., Smith, J. M. A., and Harrison, P. M. (1988) Self-assembly of apoferritin from horse spleen after reversible chemical modification with 2,3-dimethylmaleic anhydride. *Biochemistry* **27**, 4089–4096
27. Cornell, T. A., Fu, J., Newland, S. H., and Orner, B. P. (2013) Detection of specific protein-protein interactions in nanocages by engineering bipartite FlAsH binding sites. *J. Am. Chem. Soc.* **135**, 16618–16624